ASSESSMENT OF TIDAL ENERGY RESOURCE IN THE STRAIT OF GIBRALTAR

SITE 1: CONTINENTAL SHELF OFF TARIFA

PHYSICAL OCEANOGRAPHY GROUP
UNIVERSITY OF MALAGA

1. Project description

1.1 Involved parties

Tidal resource assessment is carried out by the Physical Oceanography Group of the University of Malaga (SPAIN) in the frame of the Research Project "**Mapas de flujos de energía en el Estrecho de Gibraltar para su aprovechamiento como fuente de energía renovable" (FLEGER) P08-RNM-03738** funded by the Regional Govern of Junta de Andalucía (SPAIN).

1.2 Previous work

No pervious resource assessment works has been carried out in the Strait of Gibraltar, the proposed site of the present resource assessment.

1.3 Objective and nature of resource assessment

1.3.1 General

The objective of this study is to evaluate the marine currents potential, as source of renewable energy, in the area of the Strait of Gibraltar. The main aim of the draft methodology followed in this study is to measure and describe this resource in order to understand the potential for the power extraction of an array of Technical Energy Conversion System (TECS) and to ensure that the tidal resource available is not over-extracted.

The Strait of Gibraltar (see Figure 1) is the only connection between the eastern North Atlantic Ocean, where tidal ranges are in excess of 2 m, and the western Mediterranean Sea, where they are very small. As a result, tides in the Strait move huge volumes of water back and forth to couple both regimes, originating intense tidal currents. Therefore, this is a potential development area that deserves to be investigated.

1.3.2 Resource assessment stage

This study will be focused on the northern continental shelf of the Strait of Gibraltar. One array was deployed off Tarifa (See figure 1), at a mean depth of 100 m, to measure marine currents. Accordingly to the project characteristics, the study is considered to be in a "site assessment-pre-feasibility" stage.

1.4 TECS characteristics

1.4.1 General

No specific TECS has been considered in this study so the horizontal axis turbine will be used to compute the amount of energy liable to be extracted. It is the most advanced tidal stream technology available at present.

1.4.2 Generic characteristics

- Maximum rotor diameter. The maximum diameter for a standard horizontal axis turbine is currently limited to 25 m.
- Top clearance. A 10 m top clearance is used to allow for recreational activities and to minimize turbulence and wave loading effects on the TECS, as well as damage from floating materials.
- Bottom clearance. A 5 m bottom clearance is defined to minimize turbulence and allow for potentially TECS-damaging materials that are moved along the seabed by the currents.
- Device spacing. The lateral spacing between devices would be 62.5 m (2.5 times the rotor diameter) whereas the downstream spacing would be planned to be 250 m (10 times the rotor diameter). The devices would be positioned in an alternating downstream arrangement to take the maximum profit from the incoming tidal energy.

1.5 Extent of array

The project is planned for testing purposes so just a few rows of TECS within a small-scale farm are considered to be installed. This configuration will have a rated capacity between 3 MW and 20 MW. Details about the location and number of TECS to be installed will be provided in subclauses 1.7 and 5.2.

1.6 Site conditions

1.6.1 Bathymetry

Data Available

The bulk of data used in this project come from the bathymetric charts developed by the Spanish Institute of Oceanography (IEO) in the studying area. Specifically, data were taken from *Sanz et al*., [1991][1] and have been complemented with Gebco (5th edition) database[2] in order to obtain a more detailed bathymetry of the northern continental shelf of the Strait.

Site bathymetric issues

The Strait of Gibraltar is a narrow and shallow channel 60 km long and 20 km wide, characterized by a complex system of contractions and sills. The bathymetry progressively decreases entering in the Strait, from near 2000 m in the Alboran sea (the sub-basin adjacent to the Strait in the Mediterranean Sea side), to about 800-900 m in the eastern entrance of the strait, the section between Gibraltar and Ceuta. West of this section the Strait gets narrower in the so called Tarifa Narrows (TN) characterized by a bathymetry of more than 800 m until reaching the minimum width section next to Tarifa (about 14 km). Further west, the bottom

---

[1] *J. L. Sanz, J. Acosta, M. Esteras, P. Herranz, C. Palomo y N. Sandoval. Prospección geofísica del Estrecho de Gibraltar (Resultados del programa Hércules 1980-1983). Publicaciones especiales del Instituto español de oceanografía, no7, 1991*

[2] *General Bathymetric Chart of the Oceans, Digital Atlas (GDA). Canadian Hydrographic Service, Ottawa, Canada, under the joint authority of the International Hydrographic Organization (IHO) and the Intergovernmental Oceanographic Commission (IOC), 1978-1982*

abruptly raises reaching the minimum depth of the whole Strait (290 m) at the Pta. Camarinal section, determining the so called Camarinal Sill. More to the west, the presence of a submarine ridge called Majuan Bank (MB) divides the outflowing cross-section into two channels. The northern channel has a maximum depth of only 250 m; just south of the bank, the southern channel reaches the relative minimum depth of 360 m in the topographic point called Espartel Sill (ES).

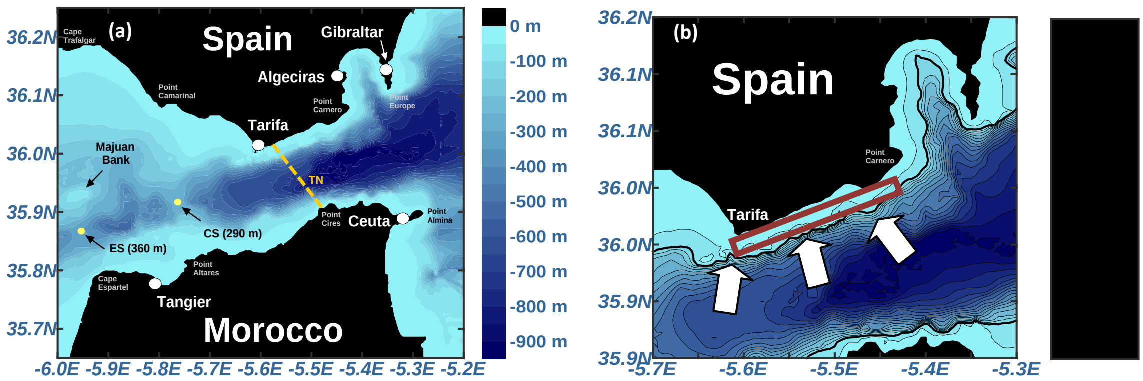

Figure 1. Map of the Strait of Gibraltar (a) showing the main topographic features: the main sills of Camarinal (CS) and Espartel (ES) and Tarifa narrows (TN). (b) Details of the Spanish continental shelf showing the areas suitably homogeneous for TECS installation (red rectangle) and steep gradients (white arrows).

The area of interest is placed in the northern continental shelf of the Strait of Gibraltar, between Tarifa and Point Carnero (red rectangle in figure1.b); in a plateau with a sandy seafloor that reaches a maximum depth of 100 m. Following to the south, the bottom abruptly fall reaching depths greater than 500 m in the main channel.

1.6.2 Oceanography

The mean circulation within the Strait of Gibraltar is described as an inverse estuarine circulation (*Stommel and Farmer,* 1953)[3], characterized by a two-way exchange, with an upper flow of about 1 Sv (1 Sv = 10^6 m^3 s^{-1}) of relatively fresh (Salinity of 36.2 psu) and warm Atlantic water spreading in the Mediterranean basin and a lower flow slightly smaller of cold and salty Mediterranean Water (Salinity of 38.4 psu) spreading in the North Atlantic Ocean. The excess of evaporation over precipitation and river runoff, along with buoyancy losses in the Mediterranean basin drive this two-layer baroclinic exchange in the Strait. It presents a high variability with strong fluctuations at semidiurnal frequency and less important but non negligible subinertial fluctuations in the range of few days to few weeks linked to meteorological forcing (*Candela et al.*, 1989; *García-Lafuente et al.*, 2002)[4], and also seasonal and interannual variations.

---

[3] *Stommel, H., and H. Farmer, Control of salinity in an estuary by a transition, J. Mar. Res., 12, 13– 20 (1953).*

[4] *Candela, J., C. Winant, and H. L. Bryden, Meteorologically forced subinertial flows through the Strait of Gibraltar, J. Geophys. Res., 94,12,667– 12,674 (1989); Garcíaa-Lafuente, J., E. Alvarez-Fanjul, J. Vargas, and A. Ratsimandresy, Subinertial variability through the Strait of Gibraltar, J. Geophys. Res., 107(C10), 3168, doi:10.1029/2001JC001104 (2002).*

Mean currents in the northern continental shelf flow eastwards spreading into the Mediterranean Sea. This general pattern is modified by tidal dynamics in the following way: the Atlantic inflow is enhanced during ebb tides, when tidal currents flow into the Mediterranean basin, whereas it is much reduced during flood tide (westward moving). Current inversions may take place during this part of the tidal cycle spreading depending on the relative intensity of tidal currents respect to the mean current. This fact should be taken under consideration when a specific TECS is previously identified to undertake the resource assessment.

1.6.3 Tidal range

Tidal range has been obtained from data collected by two tide gauges placed at Tarifa and Ceuta (Figure 2) in order to have an overview of the barotropic tidal behavior in the area. Data have been taken from the tide gauge network program developed by the Spanish institute of Oceanography (IEO). The Ceuta station belongs to the Mediterranean Sea Level Observing System (MEDGLOSS).

One year-long time series were used to investigate the seasonal variability as well as the spring-neap tidal cycles at both locations.

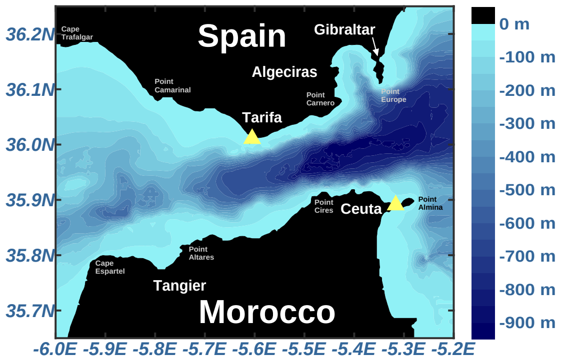

Figure 2. Map of the Strait of Gibraltar showing the locations of the two tide gauges.

Annual profile

Figure 3 shows the tidal range annual profile recorded at Tarifa (upper panel) and Ceuta (lower panel), respectively, with sampling interval of 20 minutes. Tides in the Strait are typically semidiurnal, showing two highs/lows per day, although with differences in heights due to the diurnal inequality, related to changes of the declination of the Moon and other non astronomical factors like the size, depth, and topography of ocean basins, shoreline configuration, and meteorological conditions. This fact will be addressed in the *daily profile* subclause.

Tidal records present a typical fortnightly cycle of spring-neap tides, with higher mean sea level (MSL) variability at Tarifa due to its westernmost location. This implies a greater potential energy production that makes this site more suitable for the installation of TECS. Maximum ranges of about 1.3 m are observed during the most energetic spring tides at Tarifa whereas minimum ones lower than 0.4 m take place during the weaker neap tides. The fortnightly cycle will be fully addressed in the *monthly profile* subclause.

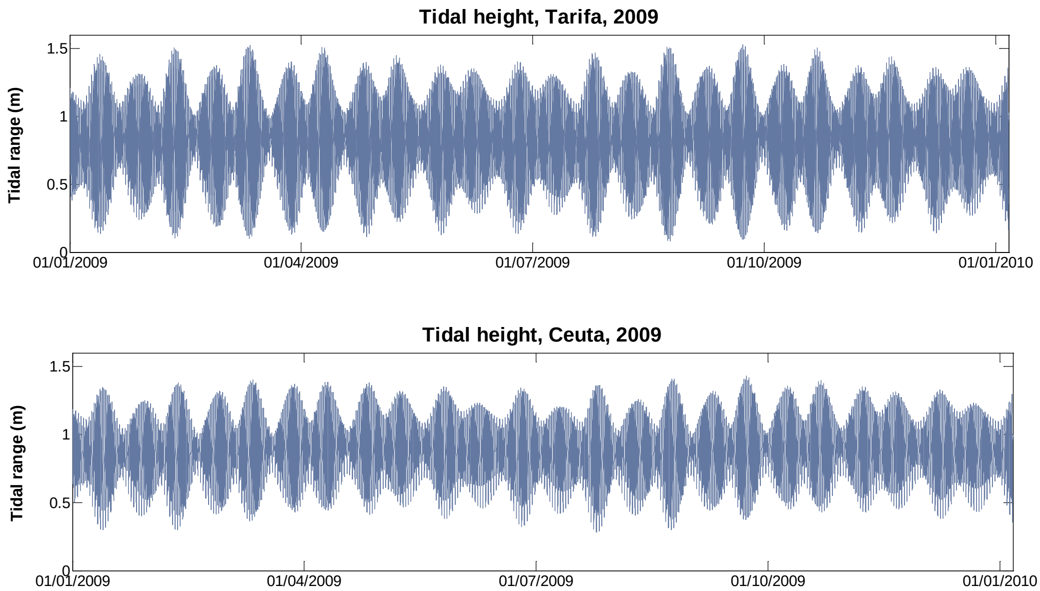

Figure 3. Tidal range predicted in Tarifa (upper panel) and Ceuta (lower panel) during 2009

Monthly MSL averages (table 1) show a seasonal signal that peaks in late summer at Tarifa and reaches minimum values in early winter. This seasonality is also observed at Ceuta, showing amplitude much higher than that obtained at the northern limit of the Strait. Moreover, a time lag of about two months is also observed as a result probably of the wind regime. Months of May and September has been taken as representative of the annual MSL average at Tarifa and Ceuta, respectively. Those months will be used to estimate the average power density during the year.

Month	Mean value (m) Tarifa	Max. value (m) Tarifa	Mean value (m) Ceuta	Max. value (m) Ceuta
January	0.7884	1.4570	0.8496	1.3460
February	0.7893	1.5060	0.8569	1.3790
March	0.7866	1.5250	0.8819	1.4030
April	0.7880	1.5080	0.8970	1.3860
May	0.7896	1.4470	0.8840	1.3520
June	0.7909	1.4020	0.8647	1.3420
July	0.7933	1.4700	0.8488	1.3630
August	0.7940	1.5090	0.8567	1.4060
September	0.7920	1.5300	0.8819	1.4290
October	0.7902	1.5060	0.8986	1.3960
November	0.7882	1.4390	0.8894	1.3500
December	0.7852	1.3630	0.8627	1.3300
Average	**0.7896**	**1.4718**	**0.8713**	**1.4290**

Table 1. Tidal range monthly means and maximum monthly values at Tarifa and Ceuta.

Monthly profile

The average months extracted from Table 1 are used here to describe the spring-neap tidal cycle. Figure 4 show a 30-day plot of the tidal height at the sites of Tarifa (upper panel) and Ceuta (lower panel), respectively.

Maximum ranges of about 1.3 – 1.4 m are observed at Tarifa during the spring-tide periods, being reduced by around 50 % during the most energetic neap tides (80 % for the weaker ones), this having impact on the intensity of tidal currents. Maximum MLS variability takes place in 7-9th and 24-26th may, so maximum tidal velocities are expected to be reached around those days at this location. On the other hand, the site of Ceuta presents a spring-neap cycle weaker than that observed at Tarifa, with maximum amplitudes lower than 1.2 m reached in 5-7th and during the most energetic tidal periods. As a consequence, lower tidal currents are expected at this location.

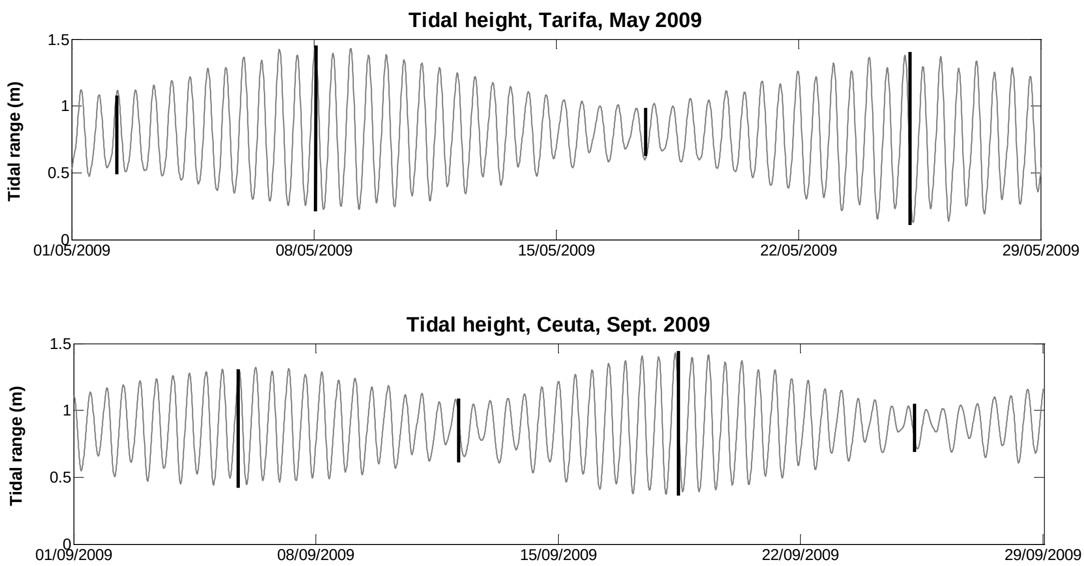

Figure 4. 30-day profile at Tarifa (upper panel) and Ceuta (lower panel).

Daily profile

Figure 5 presents the daily tidal profile at Tarifa (upper panel) and Ceuta (lower panel), respectively, during the most energetic spring-tide period of the average month. The mean height has been removed from the tidal records to show the MSL anomalies. As it was aforementioned, tides in the Strait present a mixed semidiurnal cycle with two highs/lows per day with different amplitudes. It is more evident in records collected at Tarifa (upper panel of Figure 5) due to the higher energy of tides at this location. As a result, tidal currents (and therefore the energy liable to be extracted) are expected to peak at different values in each tidal cycle, this involving that absolute maximum velocities are reached once a day.

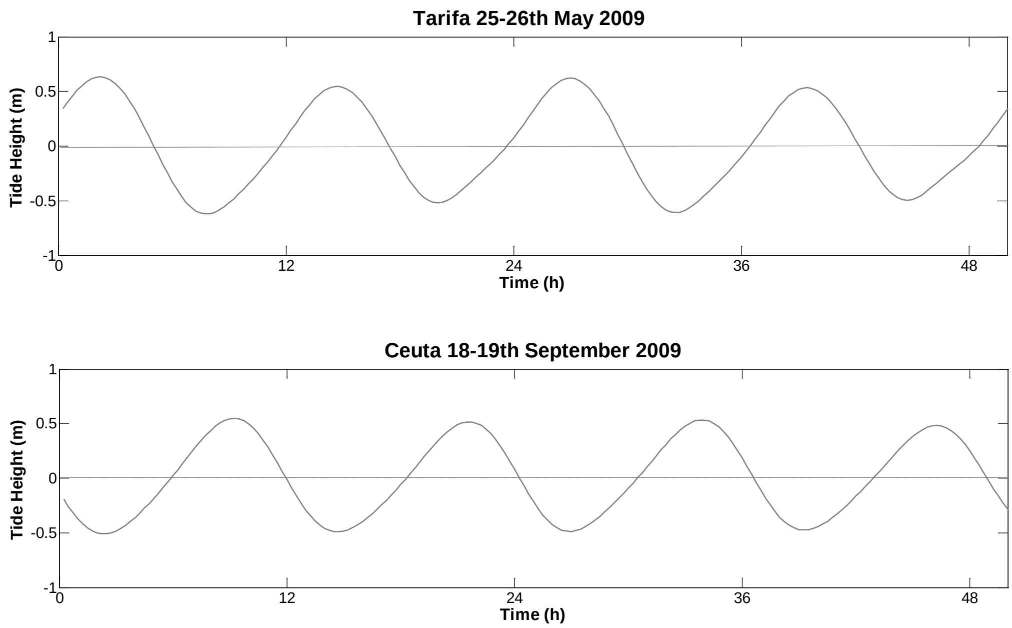

Figure 5. Mean-free tidal daily profile at Tarifa (upper panel) and Ceuta (lower panel).

1.6.4 Tidal currents

Data Available

Velocity time-series come from a static survey deployed in ending May 2009 in the area of Tarifa Narrows (see Figure 6) in the frame of the Spanish-funded FLEGER Project. One-month length velocity records were subjected to classical harmonic analysis (*Foreman,* 1978)[5] and the main diurnal and semidiurnal tidal constituents were identified to predict the tidal currents for the MSL average month of May. This data will be used to correlate tidal currents and MSL variability at Tarifa. The details of the oceanographic static survey will be provided in the *Results presentation* clause.

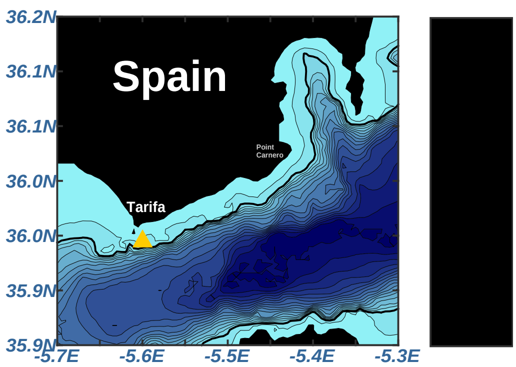

Figure 6. Map of the Strait of Gibraltar showing the topographic features and the location of the array (yellow triangle).

Correlation between tidal height and tidal currents

Tidal currents and MSL anomalies predicted during the most energetic spring-tide period of May at Tarifa have been compared to show the relationship between the barotropic tide and its associated currents. Figure 7 show the MSL anomaly and the tidal current at 45 m depth computed for the 25th May 2009. This depth could be representative of the entire water

---

[5] *Foreman, M. G. G., Manual for tidal currents analysis and prediction. Pacific Marine Science Report 78-6, Institute of Ocean Sciences, Patricia Bay, Sidney, BC, 57pp. 1978*

column (maximum depth of 100 m). At first glance, tidal currents correlate well with tidal range so a simple analysis of the tidal range might allow a rough prediction of the currents throughout the year. On the other hand, the peak value of tidal currents takes place 6 hours after highs due to the standing-wave character of the barotropic tide in the Strait of Gibraltar. If this time-shift is considered, a maximum correlation of around 80 % is obtained.

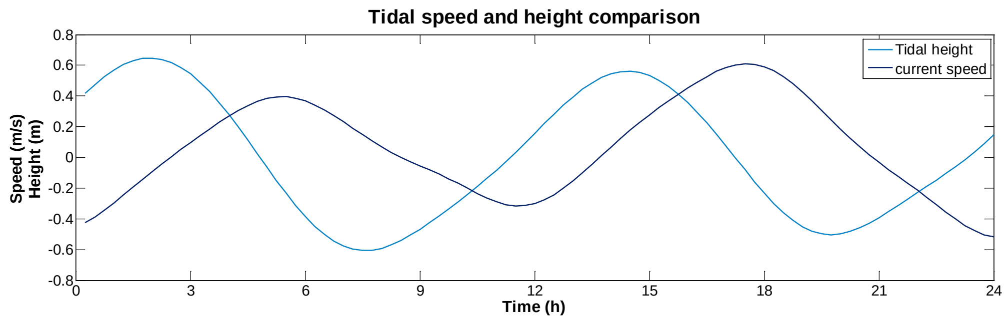

Figure 7. Tidal current speed (blue line) and mean sea level anomaly (pale-blue line) computed for the 25th May 2009 at Tarifa. Positive velocity values denote eastward moving and negative velocity values indicate westward flowing.

1.7 Physical boundaries of assessment

Boundaries of the detailed resource assessment area were identified from the bathymetric charts reported in subclause 1.6. Since no specific TECS has been considered in this study, all the sites of the northern continental shelf of the Strait in the area of Tarifa with a suitable depth range between 20 and 100 m should be considered. This depth represents the vertical limit of the Spanish continental platform. Since this project is planned for testing purposes, a small area has been chosen to potentially install the farm of TECS (red rectangle in Figure 8b). It has a total length of 925 m (0.5 nautical miles) and a width of 370 m (0.2 nautical miles), this giving a total area 342.250 m^2. This area will be used in subclause 5.2 to estimate the tidal resource assessment by using the farm method.

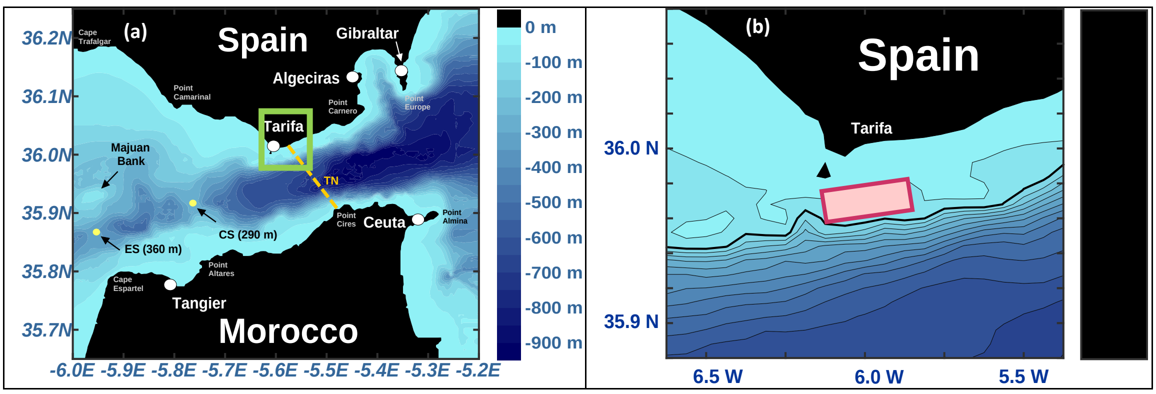

Figure 8. Map of the Strait of Gibraltar (a) showing the main topographic features. Green rectangle denotes the highlighted area where tidal resources are planned to be extracted. (b) Detail of the Spanish continental shelf off Tarifa where the mooring array were deployed. Red rectangle denotes the area considered for the TECS array installation.

2. Results presentation

2.1 Tidal harmonic analysis

Classical vectorial harmonic analysis has been performed to Acoustic Current Profiler (ADP) velocity records presented in subclause 1.6.4 (see Figure 6). The length of the time-series (35 days) let us to resolve 35 tidal constituents that will be used to predict the tidal currents at this site over any given period. The constituents extracted include the 10 most significant ones defined in standard order[6]. Details of the mooring and datasets will be provided in the *static survey* subclause.

Figure 9 presents the vertical profile of tidal currents associated to M_2. This tidal constituent exhibits the highest amplitude and also turns out to be the most stable in terms of signal/noise ratio (snr). Therefore, It is the most suitable to describe the tidal flow at semidiurnal frequencies in the area of interest. Maximum amplitudes greater than 0.55 m s^{-1} are observed in the upper part of the water column, which progressively decreases with depth until reaching a minimum value lower than 0.3 m s^{-1} 18 m above the sea floor due to frictional effects. No-data close to bottom are available, although M_2 tidal velocity is expected to reduce to zero in the bottom boundary layer. On the other hand, data collected in the first 20 m of the water column have been removed from the velocity records due to the noise exerted by the sea surface, which distort the pulses generated by the ADP. Phase presents a local maximum at middle depths and decreases towards the sea surface and bottom. According to the linear theory of internal waves in a continuously stratified flow, the group velocity (the energy) has vertical propagation of different sign that phase at semidiurnal frequencies (since $N>\omega>f$). Therefore the energy propagates upwards and downwards from the depth of maximum phase towards the surface and towards the bottom.

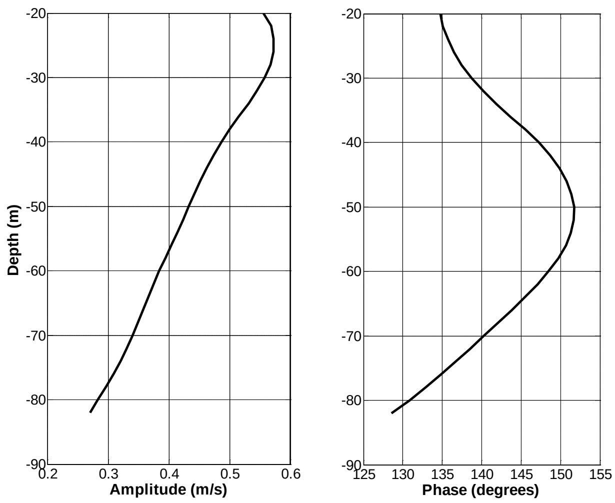

Figure 9. Mean vertical profile of the M_2 tidal constituent at Tarifa. (a) amplitude (m/s). (b) phase (degrees)

6 *Couch, Dr Scott and Jeffrey, Henry, Preliminary Tidal Current Energy Device Performance Protocol – Version 1.3, DTI, February 2007*

2.2 Hydrodynamic model

This study is based on direct observations collected in the northern slope of the Strait of Gibraltar so no hydrodynamic models for the region concerned have been considered.

2.3 Transect survey

The transect survey should be carried out during Stage 2 of the assessment around the possible location of the TECS during a typical spring tide cycle along the two days with strongest currents. The aim is to provide an overview of the spatial variation of the velocity distribution over the site. Nevertheless, no transect surveys have been undertaken because tidal current dynamics in the Strait have been extensively studied and analysed by different authors[7] during the last decades at different sites. As a result, the complicate tidal pattern in this area has been described and we have taken profit of this previous work to choose the appropriate area for TECS installation. Therefore, this study has been based on data collected by static survey deployed in the site of interest.

2.4 Static survey

The monitoring station was deployed over the northern continental shelf of the Strait of Gibraltar at coordinates 35° 59.59 'N / 005° 35.73 'W between 26th May 2009 and 1st July 2009. This station consists of an up-looking moored ADP at 100 m depth (10 m above the seafloor) that resolves 32 bins, 2-meter thick each one, and provides horizontal velocity at 32 levels every 2 minutes. Data collected by the ADP device will be used to investigate currents in the area of interest. Maximum velocities or around 2 m s^{-1} are observed for the most energetic spring-tide periods in the upper part of the water column during the ebb tide, when barotropic tidal currents flow to the east into the Mediterranean Sea. This result is in concordance with the M_2 vertical profile extracted from the harmonic analysis (Figure 9).

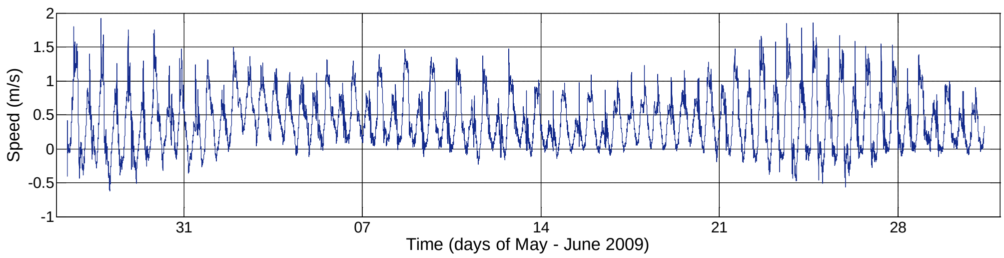

Figure 10. Depth-averaged tidal velocity (m/s) collected by the ADP device during ending May - June 2009 at Tarifa

Figure 10 presents the depth-averaged velocity profile during the whole period of data collection. Maximum velocities of around 1.5 – 2.0 m s^{-1} take place during the ebb tide of the

---

[7] *For instance García Lafuente, J., J.L. Almazán, F. Fernández, A. Khribeche, and A. Hakimi, Sea level in the Strait of Gibraltar: tides, Int. Hydrogr. Rev., LXVII (1), 111-130 (1990)*

Candela, J., C. Winant, and A. Ruiz, Tides in the Strait of Gibraltar, J. Geophys. Res., 95, 7313-7335 (1990).

most energetic tidal periods whereas currents reduce to a minimum of 0.5 – 1.0 m s^{-1} during the same part of the tidal cycle in the weaker neap tides. Diurnal inequality makes that absolute maximum values are only observed once per day. On the other hand, current inversions are observed during the flood tides (westwards moving) for the spring-tide periods reaching maximum values of -0.5 m s^{-1} (negative sign denotes currents towards the Atlantic Ocean). Those inversions take place twice per day although with different intensity due to the diurnal inequality. It is interesting to note that negative velocities are not observed during the weaker neap tides because tidal currents are not stronger enough to reverse the mean flow. As a consequence, the entire water column (or at least the most part of it) always flows into the Mediterranean basin.

All those factors will have impact on the amount of potential energy available and therefore liable to be extracted by the TECS.

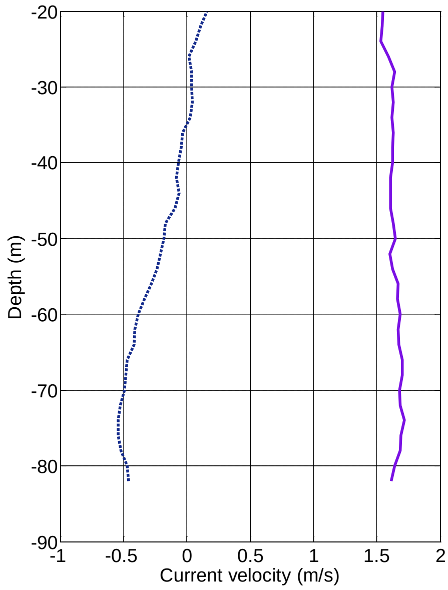

Figure 11.Vertical profile of currents observed in maximum ebb (solid line) and maximum flood (dashed line) during spring tides

To further investigate the currents variability during the spring-tide periods, Figure 11 presents two instantaneous vertical profiles collected during the ebb and flood tides in 24th June 2009. Semidiurnal tidal cycles make oscillate mean currents back and forth with a periodicity of approximately 6 hours. Total currents are barotropically enhanced during ebb tide so the entire water column is displaced into the Mediterranean Sea. When tide reverses and tidal currents flow towards the Atlantic Ocean, (in opposite direction to the mean flow), they cancel or reverse the mean currents westwards showing a vertical profile similar to that plotted in Figure 11 (dashed line). In this case a baroclinic pattern is observed with negative higher velocities in the lower half of the water column, at around 75 m depth, whereas weak positive values are still obtained close to the sea surface. This result is the consequence of the differences in velocity found along the water column. Mean currents are stronger in the upper part (see Figure 9) so they are less sensitive to the tidal forcing during the flood periods.

Finally, a fourth order Butterworth low-pass filter with a cut-off frequency of 1/3 $hours^{-1}$ was applied to the depth-averaged tidal profile presented in Figure 10 to remove instrument noise and turbulent motions, as well as the higher frequency data. Time series were filtered first forward and then backwards in time through the same filter to avoid phase shifts. Figure 12 presents both the filtered and unfiltered time series, which present an average value of 0.81 m s^{-1} and 0.82 m s^{-1} respectively.

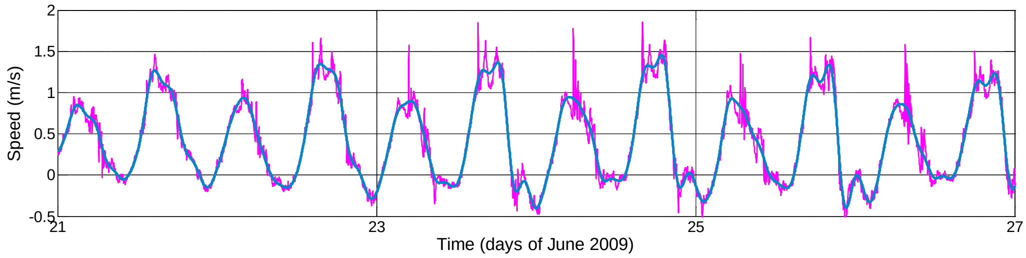

Figure 12.Comparison between filtered (pale-blue line) and unfiltered (pink line) depth-averaged tidal velocity (m s^{-1}) collected by the ADP device at Tarifa

3. Data analysis

3.1 Velocity distribution

ADP velocity records have been used to compute the velocity distribution f (U_i) of currents for the entire water column in the area of interest. A histogram analysis has been performed by using a standard interval of 10 minutes and a bin size of 0.1 m s^{-1} in order to obtain the percentage of time that the velocity falls within each bin. Table 2 presents the results obtained for some levels along the water column.

Velocity (m s^{-1})	Levels (m)							Barotropic Velocity (m s^{-1})
	20	30	40	50	60	70	80	
-1.0	0	0	0	0	0	0	0	**0**
-0.9	0	0	0	0	0	0	0	**0**
-0.8	0.0039	0	0.0039	0.0116	0.0039	0.0155	0.0077	**0**
-0.7	0.0077	0.0464	0.0309	0.0270	0.0232	0.0657	0.0734	**0**
-0.6	0.0464	0.0579	0.0734	0.1082	0.2665	0.3129	0.3477	**0**
-0.5	0.0850	0.0850	0.1661	0.2936	0.5060	0.7571	0.7223	**0.1197**
-0.4	0.2009	0.2549	0.4828	1.0043	1.6301	1.9778	1.9816	**0.2936**
-0.3	0.4288	0.5447	1.0121	2.1709	5.3500	7.1384	6.6363	**1.2013**
-0.2	0.5871	0.9155	1.8387	5.6744	10.0239	13.1644	13.8713	**2.2095**
-0.1	1.1666	1.7112	3.6233	8.5406	11.3412	13.2146	15.6405	**5.2148**
0	1.9971	3.0593	5.2341	8.9771	9.7767	10.3098	11.8240	**10.1823**
0.1	2.6228	4.2529	6.9839	8.5484	9.6493	9.7536	10.4720	**11.4416**
0.2	4.0598	5.4736	7.8994	8.8072	8.6179	8.7338	10.0858	**10.5686**
0.3	5.5431	6.1766	8.9231	9.0196	8.3166	8.3359	8.4595	**9.1587**
0.4	7.9419	8.0462	9.5488	8.0539	6.9646	6.4740	6.1380	**7.5440**
0.5	10.5338	10.6072	8.9115	7.1307	5.9912	5.1105	4.4847	**7.4668**
0.6	10.8313	10.0973	7.4127	6.1805	4.6778	3.9671	3.4881	**7.5015**
0.7	8.3166	8.2625	7.0960	4.9289	3.6156	3.3297	2.0820	**6.7483**
0.8	6.3311	6.0491	5.7092	4.0521	3.1752	2.1902	1.2361	**5.9487**
0.9	5.4890	4.9869	4.7087	3.1945	2.7851	1.6069	0.8228	**3.5885**
1.0	4.5465	3.8435	3.6349	2.6731	2.3486	1.3018	0.6374	**2.9357**
1.1	3.7353	3.6194	3.3143	2.6769	1.6185	0.9696	0.3592	**3.4108**
1.2	3.6156	3.8358	2.7735	2.1748	1.2245	0.5060	0.2897	**2.2790**
1.3	4.5581	3.7044	2.0550	1.8541	0.8769	0.3438	0.1197	**1.8348**
1.4	5.2573	4.1911	2.2945	1.6726	0.5292	0.1816	0.0657	**0.3206**
1.5	4.8671	3.9516	2.5031	1.1009	0.3940	0.0657	0.0348	**0.0309**
1.6	3.2409	2.7040	1.8812	0.7146	0.1506	0.0618	0.0386	**0**
1.7	2.0936	1.6571	0.9850	0.2047	0.0502	0.0270	0.0464	**0**
1.8	0.9734	0.9309	0.5060	0.1391	0.0502	0.0541	0.0348	**0**
1.9	0.4249	0.5987	0.2627	0.0579	0.0425	0.0309	0	**0**
2.0	0.1352	0.2434	0.1004	0.0077	0	0	0	**0**
2.1	0.0309	0.0657	0.0309	0	0	0	0	**0**
2.2	0.0077	0.0155	0	0	0	0	0	**0**
2.3	0.0039	0	0	0	0	0	0	**0**
2.4	0	0	0	0	0	0	0	**0**

Table 2. Total velocity histogram showing the percentage of time that velocity falls within each velocity interval computed from ADP records collected at Tarifa.

The percentage of time for a specific velocity bin differs for the different levels along the water column due to the baroclinic nature of currents in the area. Two different patterns arise, showing higher occurrence likelihood of negative velocities (westward) in the deeper layer close to bottom, whereas positive velocities (eastwards) occur particularly in the upper part of the water column, with higher values as one move upwards. The exceedance curves associated to those distributions are plotted in Figure 13. Velocity distributions present maximum occurrence likelihood within the velocity bin of -0.2 m s^{-1} (around 14 % of total time) in the lower half of the water column (blue lines) showing a total time of negative values higher than 30%. This percentage progressively diminishes towards the sea surface at the same time that the occurrence likelihood of positive velocities rises up. Maximum values are obtained within the velocity bin of 0.6 m s^{-1} (around 11% of total time) at 20 m depth, according to the vertical pattern presented by the M_2 tidal constituent. Moreover, a relative maximum of around 5% of total time takes place within the velocity interval of 1.4 m s^{-1} being probably related to the higher tidal velocities achieved during the spring tide periods.

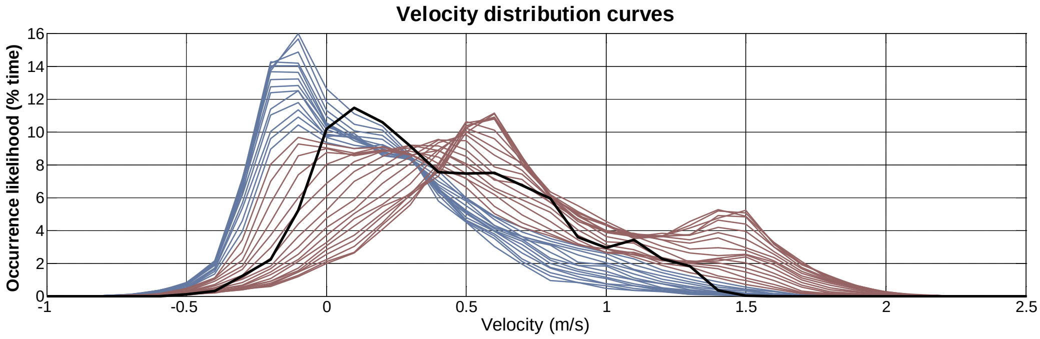

Figure 13.Velocity distribution curves for the entire water column at the mooring location. Blue lines represents velocity data collected between 56 and 82 m depth whereas red lines denote velocity data recorded between 20 and 54 m depth. Black line shows the barotropic velocity distribution.

3.2 Maximum velocities

ADP records available have been used to compute the Mean Spring Peak Velocity (V_{MSP}) for the area of interest. V_{MSP} is taken as the peak tidal velocity (observed at a mean spring tide) that has been reached for 10 minutes during one month. If velocity time series are longer than one month, the average V_{MSP} must be estimated to obtain the maximum velocity that would occur during an average month. In this case, just one month of data is available so only one V_{MSP} will be provided. On the other hand, V_{MSP} will be given only for one particular depth[8], although velocity distribution curves computed from the histogram analysis make necessary to estimate two V_{MSP}, for both the upper and lower half of the water column. Velocity data collected at 20 m depth have been taken as representative for the upper part of the water column, where a V_{MSP} value of 2.1 m s^{-1} is obtained. On the contrary, V_{MSP} diminishes until 1.4 m s^{-1} (during ebb tides) at 80 m depth due to the generalized current inversions that take place in the lower part of the water column each tidal cycle. In this case, a V_{MSP} = -0.6 m s^{-1} is observed during the flood tidal periods, when tidal currents spread into the Atlantic Ocean.

[8] *Traditionally this depth has been taken to be at 5 m below the surface due to Admiralty measurement methods; however, it may be defined at any depth or on a depth-averaged basis.*

3.3 Tidal range

Tidal range over the period when ADP datasets are available has been reported in Figure 3 (upper panel) and Table 1; so it is not presented here. Maximum ranges oscillate around 1.3 m during the most energetic spring tides whereas minimum ones lower than 0.4 m take place during the weaker neap tides.

3.4 Tidal ellipse

Tidal ellipses are required for TECS that are not able to extract energy from all directions (at different times) in order to determine the optimum orientation. Figure 14 shows the inclination of the M_2 tidal ellipse in the northern continental shelf of the Strait of Gibraltar off Tarifa. Semi-major axis presents an inclination of 5 degrees close to the sea surface (ENE-WSW direction) and progressively rotates in an anti-clockwise sense as we move downwards until reach a maximum inclination of 17 degrees between 45 and 65 m depth, which roughly coincides with the typical inclination of the axis of the Strait. Further deep the inclination diminishes until reach minimum values of around 11 degrees close to bottom. Furthermore, the topographic constriction exerted by the Strait to currents makes them to be approximately bidirectional, so the flood and ebb tides are at 180° ± 10°to each other. This is an important issue to determine the optimum orientation of the TECS for energy extraction, above all if they are not able to extract energy from all directions.

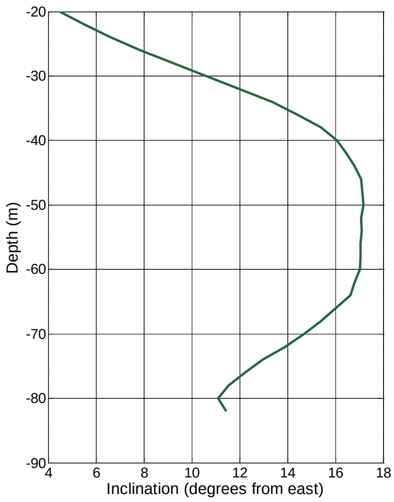

Figure 14. Vertical distribution of the inclination (degrees) of the M_2 tidal ellipse extracted from the harmonic analysis performed to the ADP velocity records collected off Tarifa.

3.5 Power density

The average power density (APD) available across the surface area where the array would be installed (see figure 6) will be computed here from the time series of the measured velocity distributions $f(U_i)$ presented in subclause 3.1. APD is calculated according to:

$$APD = \frac{1}{2} \cdot \rho \cdot \sum_{i=1}^{N_B} \left(U_i^3 \cdot f(U_i) \right) = \frac{1}{2} \cdot \rho \cdot V_{rmc}^3 \qquad (\mathrm{W\ m^{-2}}) \qquad (1)$$

Where U_i is the central value of the i^{th} bin, ρ is the water density (Kg m^{-3}), and V_{rmc} is the root mean cubed velocity, to be calculated with the equation below:

$$V_{rmc} = \sqrt[3]{\sum_{i=1}^{N_B} \left(U_i^3 \cdot f(U_i) \right)} \qquad (\mathrm{m\ s^{-1}}) \qquad (2)$$

Since two different velocity distribution patterns have been identified in the area of interest, V_{rmc} has been estimated by using the velocity distributions obtained both in the upper and lower half of the water column, at 20 m and 80 m respectively. A root mean cubed velocity (V_{rmc}) of 4.71 m s^{-1} was obtained at 20 m depth, where strong currents take place. If we assume a mean density ρ = 1027.50 Kg m^{-3} in the upper part of the water column, we obtain an APD of 53.68 kW m^{-2}. On the other hand, V_{rmc}= 1.82 m s^{-1} was estimated at 80 m depth, this providing an APD equal to 3.10 kW m^{-2} in the lower part of the water column, if a mean density of ρ = 1027.86 Kg m^{-3} is considered. Density values have been taken from the MEDAR/MedAtlas Database[9] for the area of interest.

Moreover, velocity distribution at middle depths (hub height of 50 m) has been also used to compute the root mean cubed velocity. This depth has been taken as representative of the entire water column. A *mean value* of V_{rmc}= 3.31 m s^{-1} was obtained for the entire water column that translates in an APD value of 18.63 kW m^{-2} when considering a mean density of 1027.70 Kg m^{-3}. Results are summarized in Table 3.

Depth (m)	V_{rmc} (m s^{-1})	Density (Kg m^{-3})	ADP (kW m^{-2})
20	4.71	1027.50	**53.68**
50	3.31	1027.70	**18.63**
80	1.82	1027.86	**3.10**

Table 3. ADP (W m^{-2}) computation at the site where the ADP device was installed for three velocity distributions for the upper (20 m), middle (50 m) and lower (80 m) parts of the water column.

3.6 Comparison of model with static field survey

As it was aforementioned in subclause 2.2, this study is based on direct observations only. Therefore, there are not model outputs liable to be compared to the actual data from the static field survey.

3.7 Comparison of static field survey and model with transect field survey

No transect field surveys has been carried out in this study so any comparison can be performed.

3.8 Uncertainty analysis

Velocity records used in this study have been collected by an ADP device that senses the full 3D velocity with three beams, all pointed in different directions. Each beam is slanted at 25° relative to the vertical, and equally distributed around a circle. Doppler current sensors use large transducers (relative to the wavelength of the sound) to obtain narrow acoustic beams (3 degrees width). Narrow beams are essential for obtaining good data.

[9] *MEDAR Group (2002), MEDATLAS/2002 database. Mediterranean and Black Sea database of temperature salinity and biochemical parameters. Climatological Atlas. IFREMER Edition.*

Velocity measured by the device is an average of many velocity estimates (called *pings*). The uncertainty of each ping is dominated by the *short-term error* and the measurement uncertainty can be reduced by averaging together many pings. There is a limit to how much one can reduce the velocity uncertainty: the *long-term bias* that depends on internal signal processing, especially filters. The long-term bias in the device used here is typically a fraction of 1 cm s^{-1}. The device software predicts errors based on the short-term error of a single ping and the number of pings averaged together. The short term error of a single ping depends on the size of the transmit pulse and the measurement volume, and it depends on the beam geometry. Beams parallel to the dominant flow will have smaller short-term errors than beams at a steep angle relative to the flow. Averaging multiple pings reduces errors according to the formula:

$$\sigma V_{mean} = \frac{\sigma V_{ping}}{\sqrt{N}} \tag{3}$$

Where σ is standard deviation and N is the number of pings averaged together.

3.9 External effects on tidal current speed

Velocity data used in this study come from ADP records collected by a static survey moored in the northern continental shelf of the Strait of Gibraltar. Therefore, datasets include the time variability induced by different external factors like winds, atmospheric pressure and bathymetry forcing. All of them have influence on currents observed in the area.

4. Mean annual electrical power

4.1 Power curve

Once the velocity distribution in the area of interest has been estimated, it can be applied to the TECS' power curve to compute the annual energy output.

Since no specific TECS has been chosen, a generic device will be used for this purpose. Some of its generic characteristics were described in subclause 1.4. The other characteristics required are as follows:

- Power generated in each velocity bin $P(U_i)$
- Efficiency of the device (η_R)
- Rated velocity
- Electrical efficiencies

The rotor efficiency (η_R) can be considered to rise from 38 % at cut-in speed to reach 45 % at the rated velocity. This velocity can be taken as 71 % of the V_{MSP} at the hub height. In this case, the mean spring peak velocity has been obtained at two different depths, as explained in subclause 3.2 so; two different values will be given for the upper and lower half of the water column. The cut-in velocity is the minimum velocity required for device operation and is assumed constant at 0.5 m s^{-1}. This assumption greatly simplifies the analysis and does not impose significant limitations on accuracy, since the available energy from marine currents at velocities below 0.5 m s^{-1} is usually less than 5 % of the total available energy. Finally, the average powertrain efficiency (η_{PT}) can be considered to be 90 % for a no specific TECS.

All those parameters will be used to compute the electrical power generated in each velocity bin as follows:

$$P(U_i) = P_{AV(i)} \cdot \eta_R \qquad \text{(W)} \qquad (4)$$

where

$$P_{AV(i)} = 0.5 \cdot \rho \cdot A \cdot U_i^3 \qquad \text{(W)} \qquad (5)$$

ρ denotes the water density (Kg m^{-3}); A represents the rotor swept area (m^2); and U_i is the central velocity value of the i^{th} bin (m s^{-1}) .

Table 4 presents the calculation of the electrical power $P(U_i)$ for each velocity bin (absolute values) used in the velocity distributions computation. A V_{MSP} of 2.1 m s^{-1} and 1.4 m s^{-1} have been considered for the upper and lower parts of the water column. The rated velocities will be then 1.49 m s^{-1} and 0.99 m s^{-1}, respectively. Above these values the electrical power is assumed constant. The rotor diameter considered in this study is 25 m. This is the currently maximum diameter for a standard horizontal axis turbine. Therefore, the swept area A is 491 m^2.

	V_{MSP} = 2.1 m s^{-1}			V_{MSP} = 1.4 m s^{-1}		
Average bin velocity	**Available power**	**Rotor efficiency**	**Electrical power per bin**	**Available power**	**Rotor efficiency**	**Electrical power per bin**
U_i	$P_{AV(i)}=0.5\rho AU_i^3$	η_R	$P(U_i)= P_{AV(i)}\ \eta_R$	$P_{AV(i)}=0.5\rho AU_i^3$	η_R	$P(U_i)= P_{AV(i)}\ \eta_R$
(m s^{-1})	**(kW)**	**%**	**(kW)**	**(kW)**	**%**	**(kW)**
0	–	–	–	–	–	–
0.1	0.25	0	**0**	0.25	0	**0**
0.2	2.02	0	**0**	2.02	0	**0**
0.3	6.81	0	**0**	6.81	0	**0**
0.4	16.14	0	**0**	16.15	0	**0**
0.5	31.53	38	**11.98**	31.54	38	**11.98**
0.6	54.49	39	**21.25**	54.50	40	**21.80**
0.7	86.52	40	**34.61**	86.55	42	**36.35**
0.8	129.15	41	**52.95**	129.20	43	**55.56**
0.9	183.89	42	**77.23**	183.96	44	**80.94**
1.0	252.25	43	**108.47**	252.33	45	**113.55**
1.1	335.74	44	**147.73**	335.86	X	**113.55**
1.2	435.89	44	**191.79**	436.04	X	**113.55**
1.3	554.19	45	**249.38**	554.39	X	**113.55**
1.4	692.17	45	**311.48**	692.42	X	**113.55**
1.5	851.34	45	**383.10**	851.65	X	**113.55**
1.6	1033.22	X	**383.10**	1033.58	X	**113.55**
1.7	1239.30	X	**383.10**	1239.74	X	**113.55**
1.8	1471.12	X	**383.10**	1471.65	X	**113.55**
1.9	1730.18	X	**383.10**	1730.80	X	**113.55**
2.0	2018.00	X	**383.10**	2018.72	X	**113.55**
2.1	2336.09	X	**383.10**	2336.92	X	**113.55**
2.2	2685.96	X	**383.10**	2686.91	X	**113.55**
2.3	3069.13	X	**383.10**	3070.22	X	**113.55**
2.4	3487.10	X	**383.10**	3488.34	X	**113.55**

Table 4. Electrical power per bin (kW) at the site of the mooring array. Estimations have been performed according to the two V_{MSP} values obtained for the upper and lower half of the water column, with densities of 1.027,50 kg m $^{-3}$ and 1.027,86 kg m $^{-3}$, respectively. A maximum rotor efficiency of 45 % is considered at the rated velocity (71 % of V_{MSP})

The power curves calculated here are not deemed to be accurate, but will be sufficient to determine whether the marine resource planned to be extracted by a tidal farm does not exceed the resource available in the continental shelf of the Strait of Gibraltar.

4.2 Mean annual electrical power

The mean annual electrical power (P_{mean}) can be obtained by combining the velocity distributions $f(U_i)$ with the average absorbed power for each velocity bin $P(U_i)$ calculated above by using the following equation:

$$P_{mean} = \sum_{i=1}^{N_B} P(U_i) \cdot f(U_i) \qquad \text{(W)} \qquad (6)$$

Where N_B is the number of bins used. Table 5 shows the computation of the mean electrical power for the two velocity distributions identified in subclause 3.1 by using the same device characteristics as described in subclause 4.1.

	V_{MSP} = 2.1 m s^{-1}			V_{MSP} = 1.4 m s^{-1}		
Average bin velocity	**Velocity occurrence likelihood**	**Electrical power per bin**	**Mean annual electrical power per bin**	**Velocity occurrence likelihood**	**Electrical power per bin**	**Mean annual electrical power per bin**
U_i	$f(U_i)$	$P(U_i)$	$P(U_i) \times f(U_i)$	$f(U_i)$	$P(U_i)$	$P(U_i) \times f(U_i)$
(m s^{-1})	%	kW	kW	%	kW	kW
0	1.9971	–	**0**	11.8240	–	**0**
0.1	3.7894	0	**0**	26.1124	0	**0**
0.2	4.6469	0	**0**	23.9571	0	**0**
0.3	5.9719	0	**0**	15.0958	0	**0**
0.4	8.1428	0	**0**	8.1196	0	**0**
0.5	10.6188	11.98	**1.27**	5.2070	11.98	**0.62**
0.6	10.8777	21.25	**2.31**	3.8358	21.80	**0.84**
0.7	8.3240	34.61	**2.88**	2.1554	36.35	**0.78**
0.8	6.3350	52.95	**3.35**	1.2403	55.56	**0.69**
0.9	5.4890	77.23	**4.24**	0.8228	80.94	**0.66**
1.0	4.5465	108.47	**4.93**	0.6374	113.55	**0.72**
1.1	3.7353	147.73	**5.52**	0.3592	113.55	**0.41**
1.2	3.6156	191.79	**6.93**	0.2897	113.55	**0.33**
1.3	4.5581	249.38	**11.37**	0.1197	113.55	**0.14**
1.4	5.2573	311.48	**16.37**	0.0657	113.55	**0.07**
1.5	4.8671	383.10	**18.65**	0.0348	113.55	**0.04**
1.6	3.2409	383.10	**12.42**	0.0386	113.55	**0.04**
1.7	2.0936	383.10	**8.02**	0.0464	113.55	**0.05**
1.8	0.9734	383.10	**3.73**	0.0348	113.55	**0.04**
1.9	0.4249	383.10	**1.63**	0	113.55	**0**
2.0	0.1352	383.10	**0.52**	0	113.55	**0**
2.1	0.0309	383.10	**0.12**	0	113.55	**0**
2.2	0.0077	383.10	**0.03**	0	113.55	**0**
2.3	0.0039	383.10	**0.01**	0	113.55	**0**
2.4	0	383.10	**0**	0	113.55	**0**
	P_{mean}		**104.30 kW**	P_{mean}		**5.43 kW**

Table 5. Mean annual electrical power (kW) at the site of the mooring array. Estimations have been performed according to the exceedance curves associated to the two patterns described for the upper and lower parts of the water column. Only positive velocities have been used so, velocity occurrence likelihood of negative values has been added to the ones obtained for the positive ones**.**

4.3 Annual energy production

For each TECS, the annual energy production (AEP) is obtained by multiplying the P_{mean} computed above by the available hours per year as follows:

$$AEP = 8760 \cdot A_V \cdot P_{mean} \qquad \text{(Wh)} \qquad (7)$$

where A_V is the availability (%) of energy liable to be extracted. If we assume an A_V of 100%, the annual energy production obtained for the two velocity distributions described are **AEP = 913.668 kWh** for the upper part of the water column and **AEP = 47.566,8 kWh** close to bottom.

5. Available and extractable energy

To estimate the marine resource at a specific site, two different methodologies can be carried out. The first method, called the farm method, estimates the amount of energy generated by an array by simply multiplying the electrical energy output for each TECS by the number of TECS that could be installed, or by calculating the electrical energy output of each TECS and summing the results. On the other hand, the flux method is used to check that the use of the farm method will not result in an alteration of the flow speeds that would have a significant adverse effect on the economics of the project or on the environment.

5.1 Site characteristics (energy extraction effects)

The channel shape and other site characteristics were described in subclause 1.6. Bathymetry strongly interacts with currents in the Strait of Gibraltar, including the northern continental shelf where the farm of TECS are planned to be installed (see Figure 8b). As a consequence, a typical friction coefficient of 2×10^{-2} is obtained for the whole area, one order of magnitude higher than that observed, for instance, in the Mediterranean basin. As a result, mean vertical current profile presents a strong reduction as we move bottomward so maximum current energy liable to be extracted is located, according to results presented above, in the upper part of the water column.

5.2 Resource assessment with farm method

The farm method is based on the concept of an array of tidal stream devices, each of which extracts an amount of energy related to the incoming energy. The resulting extracted energy is therefore purely dependent on the size and number of the devices, conversion efficiency and the packing density within the site area.

The size of the farm that could potentially be installed in the area of interest, described in subclause 1.7, will be used here to estimate the marine resource at the site of interest. We need first to determine the number of turbines that can be installed in the farm output power. According to the TECS characteristics related to device spacing presented in subclause 1.4, the number of devices (N_T) that can be installed in the area chosen to potentially install the farm, which presents a total surface of 0.34 Km^2, are 18; distributed in 3 rows of 6 TECS positioned in an alternating downstream arrangement. The total resource estimated by this method can be calculated by adding the annual mean electrical power (P_{mean}) of each device installed in the area as follows:

$$P_{farm} = \sum_{n=1}^{N_T} \frac{P_{mean}(n)}{\eta_{PT}(n)} \qquad \text{(W)} \qquad (8)$$

Where η_{PT} is the average powertrain efficiency and n is an index that represents a TECS. η_{PT} can be considered to be 90 % for a no specific TECS. Depending on the number of different grid cells for which a velocity distribution is available, this formula is in practice hard to apply for each device, as it would mean that each device would be designed with a different rated power to best fit the velocity distribution. This is unlikely to be the best method in practice as economies of scale would normally be lost. The devices would hence normally be grouped in areas of similar velocity distribution. As a result, a small area of hardly one squared kilometer has been chosen to carry out this study, since velocity distributions are available at only one specific site.

If we assume that the velocity distribution at the site where the ADP device was moored (described in subclause 3.1) is representative for the entire area considered for TECS installation; and devices are deployed at a nominal depth of 20 m to take profit of the maximum incoming energy, the total resource extracted by the 18 TECS and estimated with this method will be **2.086 kW**.

5.3 Resource assessment with flux method

The flux method is based on the calculation of the incoming kinetic energy flux through the frontal cross-sectional area of the flow channel. The resulting available resource estimate is independent of the device type, efficiency, and packing density, taking only the energy flowing in the channel into account. The extractable portion of the resource is then estimated using a significant impact factor (SIF), to be informed by detailed hydrodynamic or other modeling. Only one velocity distribution is available at a specific site so P_{flux} will be estimated across the whole continental slope cross-sectional area off Tarifa by multiplying the average power density (APD) by the cross-sectional area of the site considered to install the TECS.

$$P_{flux} = APD \cdot A_{channel} \qquad \text{(W)} \qquad (9)$$

Where *APD* is the average power density (W m^{-2}) computed in subclause 3.5 and $A_{channel}$ is the cross-sectional area of the continental slope off Tarifa (m^2) considered in this study (342.250 m^2). If we apply this equation to the different APD values estimated according to the different velocity distributions reported for the site where the mooring array was deployed (see Table 3), the resulting incoming kinetic energy flux through the section of interest will be the followings:

Depth (m)	APD (kW m^{-2})	Area (m^2)	P_{flux} (kW)
20	53.68	342.250	**18.371.980**
50	18.63	342.250	**6.376.117**
80	3.10	342.250	**1.060.975**

Table 6. P_{flux} (kW) computation in the area considered in this study for three ADP values obtained for the upper (20 m), middle (50 m) and lower (80 m) parts of the water column.

Finally, the annual average available power ($P_{available}$) is then the product of the power flux passing through the site and the significant impact factor (SIF):

$$P_{available} = P_{flux} \cdot SIF \qquad \text{(W)} \qquad (10)$$

The *SIF* represents the percentage of the total resource at the site that can be extracted without economic or environmental effects. There is clearly only a percentage of the total energy in the continental slope of the Strait off Tarifa that can be extracted without significant alteration to flow speed. It has an important effect on the economics of energy generation in addition to possible environmental impacts.

The SIF depends on the type of site (*Bryden et al.*, 2006)[10] in the following way: in channels where the flow is governed by a head difference at either end of the channel, and the flow cannot affect the tidal elevation in the bodies of water at either end, significant effects on the flow can be noted when this percentage is around 10%. In areas where the flow has more freedom within its elevation boundary conditions, up to 50% extraction could be possible without significant effects. Anyway, those percentages are based on theoretical modeling results that need to be validated by physical experiments so there is a presently limited understanding of the SIF that makes the estimation of the Significant Impact Factor for a given site a difficult task.

As it was aforementioned, the Strait of Gibraltar connects two areas with tidal regimes of different amplitude. Differences in sea level elevation between the ends of the Strait determine the water exchanges at tidal frequencies so a SIF close to the lower limit presented above should be chosen. If we assume a SIF of 10 %, the resulting annual average available power will be the following:

Depth (m)	P_{flux} (kW)	SIF	$P_{available}$ (kW)
20	18.371.980	10 %	**1.837.198,0**
50	6.376.117	10 %	**637.611,7**
80	1.060.975	10 %	**106.097,5**

Table 7. $P_{available}$ (kW) computation in the area considered in this study for three P_{flux} values obtained for the upper (20 m), middle (50 m) and lower (80 m) parts of the water column.

[10] *Bryden, I. G., Couch, S. J., Owen, A. and Melville, G. Tidal currents resource assessment, Proceedings of the Institution of Mechanical Engineers, Part A: Journal of Power and Energy, Volume 221, Number 2 Professional Engineering Publishing, April 2006*

The power available (incoming energy) obtained for the area of interest is much higher than the power extractable obtained with the farm method (2.086 kW) even for the deeper part of the water column where the weaker currents are observed. As a result, the proposed installation of TECS will not have any significant impact on the tidal currents in the area of interest.